Molecular Therapy
Nucleic Acids
Original Article

Silencing IQGAP1 alleviates hepatic fibrogenesis via blocking bone marrow mesenchymal stromal cell recruitment to fibrotic liver

Yuehan Ma,[1,3] Na Chang,[1,3] Yuran Liu,[1] Fuquan Liu,[2] Chengbin Dong,[2] Lei Hou,[1] Changbo Qi,[1] Lin Yang,[1] and Liying Li[1]

[1]Department of Cell Biology, Municipal Laboratory for Liver Protection and Regulation of Regeneration, Capital Medical University, Beijing 100069, China; [2]Department of Interventional Therapy, Beijing Shijitan Hospital, Capital Medical University, Beijing 100038, China

IQ motif-containing guanosine triphosphatase (GTPase)-activating protein 1 (IQGAP1) is a cytosolic scaffolding protein involved in cell migration. Our previous studies suggest sphingosine 1-phosphate (S1P) triggers bone marrow (BM) mesenchymal stromal cells (BMSCs) to damaged liver, thereby promoting liver fibrosis. However, the role of IQGAP1 in S1P-induced BMSC migration and liver fibrogenesis remains unclear. Chimeric mice of BM cell labeled by EGFP were used to build methionine-choline-deficient and high-fat (MCDHF)-diet-induced mouse liver fibrosis. IQGAP1 small interfering RNA (siRNA) was utilized to silence IQGAP1 *in vivo*. IQGAP1 expression is significantly elevated in MCDHF-diet-induced mouse fibrotic livers. Positive correlations are presented between IQGAP1 and fibrosis hallmarks expressions in human and mouse fibrotic livers. *In vitro*, depressing IQGAP1 expression blocks S1P-induced motility and cytoskeleton remodeling of BMSCs. S1P facilitates IQGAP1 aggregating to plasma membrane via S1P receptor 3 ($S1PR_3$) and Cdc42/Rac1. In addition, IQGAP1 binds to Cdc42/Rac1, regulating S1P-induced activation of Cdc42/Rac1 and mediating BMSC migration in concert. *In vivo*, silencing IQGAP1 reduces the recruitment of BMSCs to impaired liver and effectively alleviates liver fibrosis induced by MCDHF diet. Together, silencing IQGAP1 relieves liver fibrosis by blocking BMSC migration, providing an effective therapeutic strategy for liver fibrosis.

INTRODUCTION

IQ motif-containing guanosine triphosphatase (GTPase)-activating protein 1 (IQGAP1), which is closely related to cell migration, is a multi-domain protein with 1,657 amino acids. Studies have shown that IQGAP1 interacts with more than 150 molecules. By conjugating to diverse proteins, IQGAP1 integrates a large number of signaling effectors to influence cell physiology, including cell migration,[1,2] cytokinesis,[3] cell proliferation,[4] apoptosis,[5] intracellular signal transduction,[4,5] vesicle transport, and cytoskeleton dynamics.[5,6] Among these functions, cell migration has been extensively researched within various cell types, such as lung fibroblast and choroidal endothelial cells.[7,8] By impacting the cellular physiological processes, IQGAP1 acts as a pivotal character in multiple diseases. In liver, IQGAP1-related researches mainly focus on hepatocellular carcinoma (HCC).[9,10] In liver fibrogenesis, a recent study reports that IQGAP1 is increased in CCl_4-induced mouse liver fibrosis and mediates inflammatory factor expression in tumor necrosis factor alpha (TNF-α)-treated LX-2 cells.[11] However, research concerning the regulatory role of IQGAP1 in hepatic fibrosis is still in great request.

Studies have confirmed that a variety of cellular components are involved in the occurrence and development of liver fibrosis,[12,13] among which bone marrow (BM) mesenchymal stromal cells (BMSCs) play an important role in deposition of extracellular matrix.[14,15] Our previous researches have illustrated that BMSCs migrate to the injured liver and are activated into collagen-producing myofibroblasts to facilitate liver fibrogenesis.[16,17] BMSC motility has attracted interest as a therapeutic target during liver fibrogenesis. Therefore, it is urgent to investigate the regulatory mechanism underlying BMSC migration to damaged liver.

Sphingosine 1-phosphate (S1P) is a kind of bioactive lipid involved in the BMSC migration during liver fibrogenesis.[18–21] S1P exerts functions as a second messenger or through extracellular excretion. After being secreted by cells, S1P binds to and activates S1P receptors (S1PRs) in an autocrine or paracrine manner, thus participating in many vital pathological and physiological processes.[22] S1PRs consist of five G-protein-coupled receptors, namely $S1PR_{1-5}$. Among these five receptors, $S1PR_{1-3}$ are expressed in most tissues, including liver, while $S1PR_4$ is mainly expressed in lymphoid tissues and $S1PR_5$ in central nervous system.[23] When S1P binds to distinct receptors, different downstream signaling pathways are activated or inhibited. For instance, Rho family and phosphatidylinositol 3-kinase, closely related with cell motility, can be triggered by S1P.[24] A large number of reports have discovered that S1P is

Received 10 March 2021; accepted 15 December 2021;
https://doi.org/10.1016/j.omtn.2021.12.020.

[3]These authors contributed equally

Correspondence: Prof. Liying Li, PhD, No.10 Xitoutiao, You An Men, Beijing 100069, P.R. China.
E-mail: liliying@ccmu.edu.cn

This is an open access article under the CC BY-NC-ND license (http://creativecommons.org/licenses/by-nc-nd/4.0/).

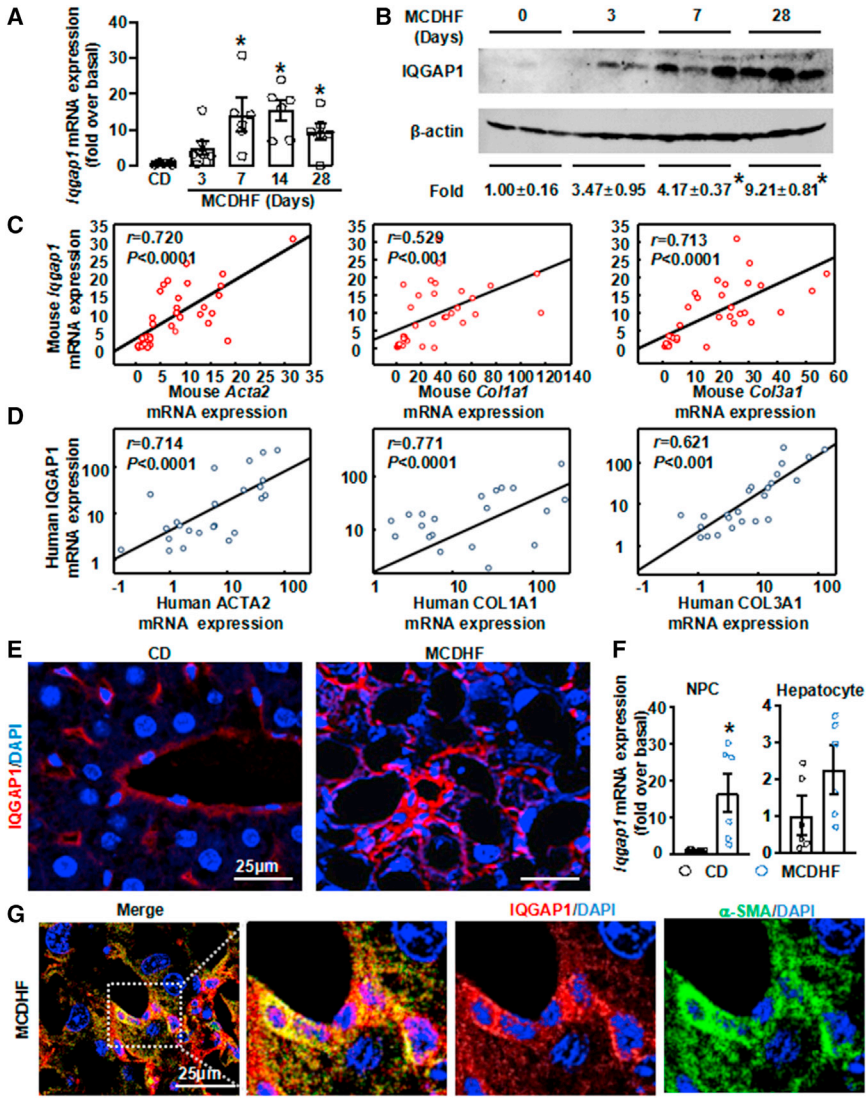

Figure 1. The expression and localization of IQGAP1 during MCDHF-diet-induced liver injury

Liver injury models were induced by methionine-choline-deficient and high-fat (MCDHF) diet. (A) *Iqgap1* mRNA expression was studied in mouse livers with MCDHF diet feeding. (B) The protein level of IQGAP1 was detected in MCDHF-diet-fed mouse livers. (C and D) The correlations between mRNA levels of IQGAP1 and three liver fibrosis markers in mouse (C) or human (D) injured livers. (E) Immunofluorescence showed the localization of IQGAP1 in MCDHF-diet-induced fibrotic mouse livers. Scale bars: 25 μm. (F) Liver non-parenchymal cells (NPCs) (left) or hepatocytes (right) were isolated from mice fed with or without MCDHF diet. qRT-PCR was employed to detect IQGAP1 mRNA expression. (G) Representative images of immunofluorescence showed the expression of IQGAP1 and α-SMA in MCDHF-diet-induced liver fibrosis. DAPI was used for nuclear staining. Scale bars: 25 μm. Data are presented as the means ± SEM. *p < 0.05 versus control group (n = 6, per group).

an important participant during liver fibrogenesis.[25] Previous studies in our laboratory have demonstrated that there is a S1P concentration gradient between bone marrow and fibrotic liver during liver fibrogenesis, which induces BMSCs migration in $S1PR_3$-dependent manner.[26] However, the latent molecular mechanism of S1P-induced BMSC migration remains to be elucidated, so we explored whether IQGAP1 participates in S1P/$S1PR_3$-mediated BMSC migration.

In the present research, we intend to investigate the specific molecular mechanism of IQGAP1-mediating, S1P-induced migration and the effect of IQGAP1 during hepatic fibrogenesis. Our findings reveal that IQGAP1 promotes S1P-induced BMSC motility *in vitro* by translocating to plasma membrane, which is dependent on $S1PR_3$ and Cdc42/Rac1. *In vivo*, we discover that IQGAP1 is up-regulated during liver murine fibrogenesis and is positively correlated with fibrosis markers both in mouse and human fibrotic livers. Moreover, IQGAP1 small interfering RNA (siRNA) treatment *in vivo* prominently restrains BMSC recruitment to injured liver and ameliorates liver fibrosis. These data expand our comprehension of IQGAP1 regulatory effects on BMSC migration and liver fibrosis, indicating IQGAP1 acts as a potential target for treatment and even prevention of hepatic fibrosis.

RESULTS

IQGAP1 is up-regulated during murine liver fibrogenesis and positively correlated with liver fibrosis hallmarks, implying that IQGAP1 may participate in liver fibrogenesis

The liver fibrotic mouse model was established by methionine-choline-deficient and high-fat (MCDHF) diet. Liver IQGAP1 expression was dramatically up-regulated (Figures 1A and 1B). In addition, we also detected *Iqgap1* mRNA expression in bile duct ligation (BDL)-induced mouse fibrotic livers to further demonstrate the result. It is discovered that IQGAP1 expression was elevated (Figures S1A and S1B).

Then, correlation analysis was performed to further confirm the relationship between IQGAP1 and liver fibrosis markers in mouse and human livers. There were positive correlations between the expression of IQGAP1 and ACTA2 (α-smooth muscle actin [α-SMA], the marker of myofibroblasts), procollagen α 1 (I) (COL1A1) and procollagen α 1 (III) (COL3A1), respectively (Figures 1C, 1D, and S1C).

IQGAP1 is mainly elevated in liver NPCs and expressed abundantly in myofibroblasts

To further explore the expression and cellular location of IQGAP1 in liver injured tissue, immunofluorescence was performed. Compared

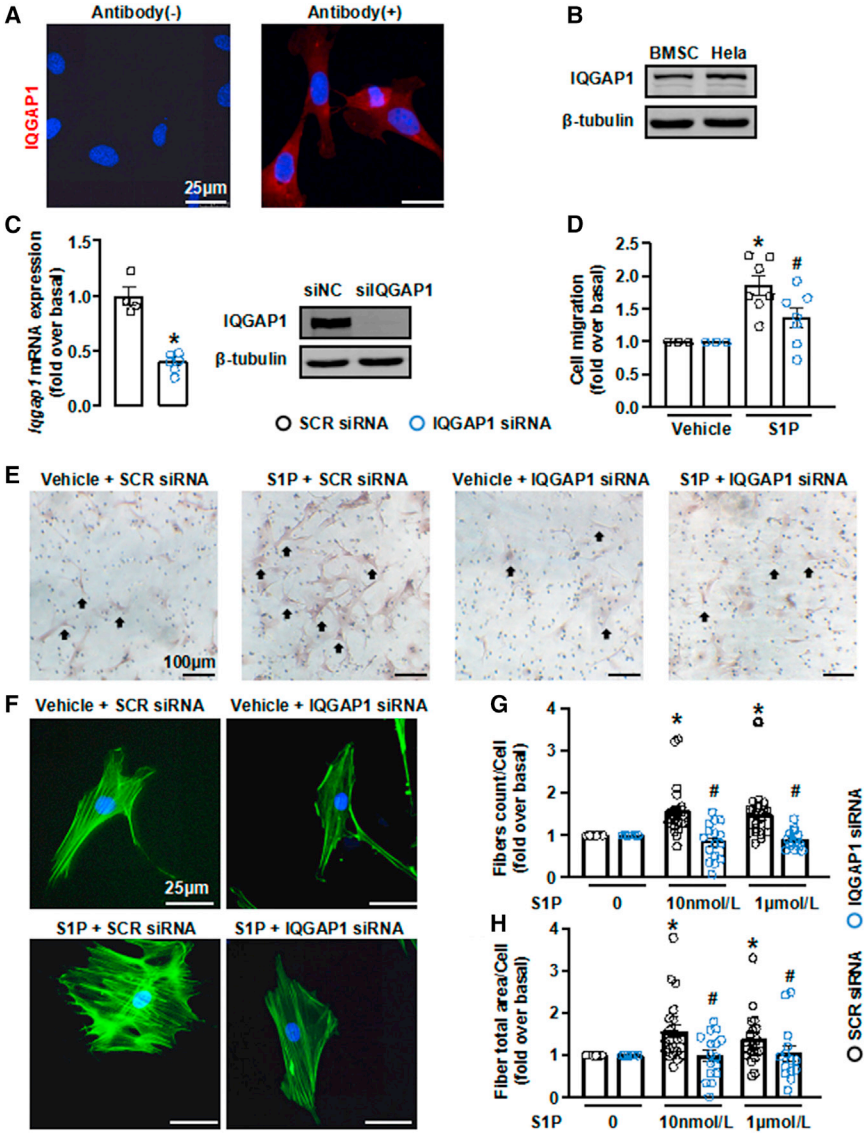

Figure 2. IQGAP1 is involved in S1P-induced migration of BMSCs

(A and B) The expression of IQGAP1 in BMSCs was detected by immunofluorescence (A) or western blot (B). HeLa cells was used as the positive control (B). Scale bars: 25 μm. (C) IQGAP1 was knocked down by small interfering RNA (siRNA) (40 nmol/L); the knockdown efficiency of IQGAP1 was studied by qRT-PCR (left) or western blot (right). (D) The migration ability of BMSCs was detected by Transwell chambers. (E) The representative images of BMSC migration. Scale bars: 100 μm. Arrow indicates migrating cell. (F) The representative images of microfilaments staining in BMSCs. Scale bars: 25 μm. BMSCs were stimulated with 10 nmol/L and 1 μmol/L S1P; the remodeling of microfilaments was examined by high-content analysis. (G and H) The fiber number (G) and fiber area (H) were analyzed by high-content analysis. Data are presented as the means ± SEM. All results were confirmed in three independent experiments at least. *$p < 0.05$ versus control group and #$p < 0.05$ versus S1P group (n = 3, per group).

with the control, the fluorescence intensity of IQGAP1 was enhanced in the liver with MCDHF diet (Figure 1E). We also found that IQGAP1 was expressed abundantly in non-parenchymal cells (NPCs) by contrast with hepatocytes. Then, we isolated hepatocytes and NPCs from mouse liver with or without MCDHF diet. Albumin (hepatocytes marker) expression was detected to examine the purity of isolated cells (Figure S1D). *Iqgap1* mRNA expression was strikingly increased in liver NPCs of mice with MCDHF diet feeding, while it was unchanged in hepatocytes (Figure 1F). Therefore, the up-regulation of IQGAP1 in injured liver tissue is mainly caused by NPCs.

Since myofibroblasts advance the development of hepatic fibrosis, the IQGAP1 expression in myofibroblasts was inspected. The results of immunofluorescence showed that myofibroblasts (α-SMA$^+$ cells) had plentiful IQGAP1 expression (Figure 1G). Previous studies have pointed out that BMSCs, which migrate from BM to damaged liver, are one of the major origins of myofibroblasts.[16,17] At the same time, S1P is an important inducer of BMSC migration during liver fibrogenesis. Therefore, we wondered whether IQGAP1 mediates S1P-induced BMSC migration.

IQGAP1 is essential to S1P-induced motility of BMSCs

Firstly, we studied whether IQGAP1 is involved in S1P-induced BMSC migration. The results of immunofluorescence and western blot displayed that IQGAP1 was abundantly expressed in BMSCs (Figures 2A and 2B). After detecting the efficiency of IQGAP1 knockdown and cell viability (Figures 2C and S2B), specific IQGAP1 siRNA was transfected into S1P-treated BMSCs. Consistent with our previous studies, BMSCs showed a prominent migratory response toward S1P. However, BMSC motility induced by S1P was predominantly inhibited when we depressed IQGAP1 expression (Figures 2D and 2E). These results suggest that IQGAP1 is involved in S1P-induced BMSC migration.

Secondly, we explored the mechanism underlying IQGAP1-involved BMSCs migration. Since cytoskeleton remodeling is prerequisite for cell migration,[27,28] we then performed high-content assay to analyze the remodeling of microfilaments (F-actin) in S1P-treated BMSCs. The results exhibited that S1P impelled the cytoskeleton remodeling of BMSCs efficaciously, as fibers number and fibers area were both

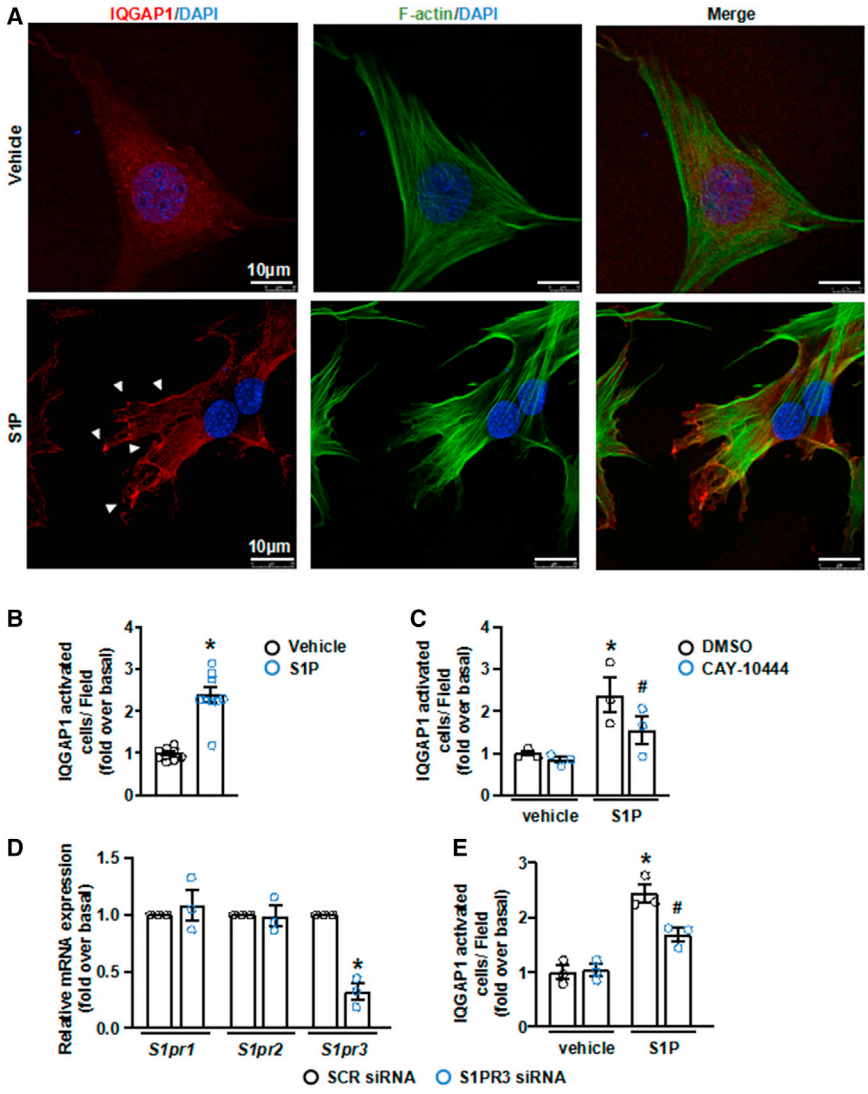

Figure 3. IQGAP1 mediates S1P/S1PR$_3$-induced cell migration by aggregating to the cytoplasmic membrane

(A) The localization of IQGAP1 in BMSCs treated with or without S1P. F-actin was also stained by FITC-labeled phalloidin. DAPI: nuclear staining. Scale bars: 10 μm. Arrowhead indicates activated-IQGAP1. (B) The number of IQGAP1-activated cells was quantified in S1P-treated BMSCs. (C) The number of IQGAP1-activated cells was quantified in S1P-treated BMSCs with preincubation of CAY-10444 (S1PR$_3$ inhibitor). (D) *S1pr3* mRNA expression was knocked down in BMSCs detected by qRT-PCR. (E) The number of IQGAP1-activated cells was quantified in S1PR$_3$-silenced BMSCs with or without S1P. Data are presented as the means ± SEM. All results were confirmed in three independent experiments at least. *p < 0.05 versus control group and #p < 0.05 versus S1P group (n = 3, per group).

increased in S1P-treated BMSCs (Figures 2F–2H). When IQGAP1 was knocked down, the remodeling of F-actin induced by S1P was significantly inhibited (Figures 2F–2H). Accordingly, we conclude that IQGAP1 is essential to S1P-induced BMSC migration and microfilament remodeling.

IQGAP1 aggregation to plasma membrane induced by S1P is dependent on S1PR$_3$

Next, we aimed to further explore the mechanism that S1P triggered IQGAP1 to exert the regulatory function in BMSC motility. RT-PCR and western blot results displayed that IQGAP1 mRNA and protein levels were not up-regulated in S1P-treated BMSCs (Figures S2D and S2E). Previous studies on epithelial cells have shown that IQGAP1 regulates cell migration and microfilaments remodeling by changing subcellular localization.[2,5] Therefore, immunofluorescence was applied to identify whether S1P alters IQGAP1 subcellular localization. The results revealed that IQGAP1 mainly localized in the cytoplasm of BMSCs without S1P treatment, while IQGAP1 partially aggregated to plasma membrane in S1P-treated BMSCs. Moreover, IQGAP1, which translocated to plasma membrane, colocalized with F-actin in S1P-stimulated BMSCs (Figures 3A and 3B). These results suggest that S1P promotes IQGAP1 accumulating to plasma membrane, where IQGAP1 colocalizes with F-actin to facilitate microfilaments remodeling in BMSCs.

In our previous research, we have reported that S1P induces migration of BMSCs in a S1PR$_3$-dependent manner, since S1P-induced BMSC migration is blocked in S1PR$_3$ siRNA-transfected or CAY-10444 (S1PR$_3$ inhibitor) pre-treated BMSCs.[26] Herein, we asked whether S1PR$_3$ is essential in the S1P-mediated membrane translocation of IQGAP1. To answer this question, we preincubated BMSCs with CAY-10444 before S1P treatment. The plasma membrane aggregation of IQGAP1 induced by S1P was significantly eliminated in CAY-10444 pre-treated BMSCs (Figure 3C). S1PR$_3$ siRNA, which specifically repressed *S1pr3* mRNA expression in BMSCs, also weakened S1P-induced IQGAP1 aggregation (Figures 3D, 3E, and S2F). Therefore, we conclude that S1P promotes IQGAP1 translocating to the plasma membrane in a S1PR$_3$-dependent manner.

IQGAP1 is activated by Cdc42/Rac1 and regulates BMSC motility in cooperation with Cdc42/Rac1

It has been confirmed that Rho family (Cdc42, Rac1, and RhoA), which bind with IQGAP1, are also fundamental regulators of cell migration.[29–31] In addition, previous research shows that Rho family and IQGAP1 combine with F-actin to regulate microfilament

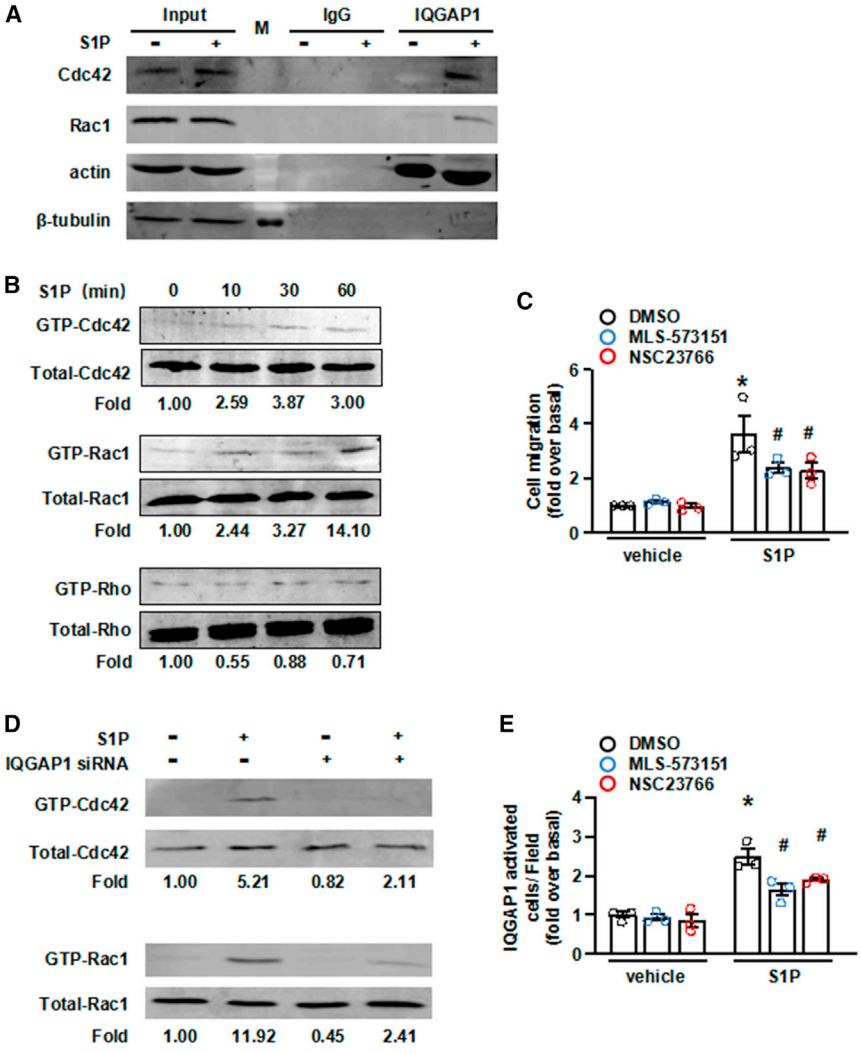

Figure 4. Cdc42 and Rac1 are involved in IQGAP1 plasma membrane aggregation

BMSCs were stimulated with S1P. (A) Immunoprecipitation showed the binding between IQGAP1 and Cdc42/Rac1/actin, respectively. (B) Rho family (Cdc42, Rac1, and Rho) activation was studied in pull-down assay upon 60 min S1P treatment. (C) The migration ability of BMSCs after MLS-573151 (Cdc42 inhibitor) or NSC23766 (Rac1 inhibitor) treatment. (D) BMSCs were pre-treated with IQGAP1 siRNA, and S1P-induced Cdc42 or Rac1 activation was detected by pull-down assays. (E) NSC23766 or MLS-573151 was employed to block the function of Cdc42 or Rac1 in BMSCs, and BMSCs were treated with or without S1P. The number of IQGAP1-activated cells was quantified. Data are presented as the means ± SEM. All results were confirmed in three independent experiments at least. *p < 0.05 versus control group and #p < 0.05 versus S1P group (n = 3, per group).

remodeling.[32] Therefore, we further investigated whether Rho family are involved in IQGAP1-mediated BMSC migration. Firstly, we considered whether Rho family and microfilament conjunct with IQGAP1 in BMSCs. Co-immunoprecipitation was performed in BMSCs treated with or without S1P. The results showed that there was almost no binding between IQGAP1 and Cdc42/Rac1 when S1P was absent, whereas in S1P-treated BMSCs, combination of IQGAP1 and Cdc42/Rac1 was boosted obviously (Figure 4A). We also observed that IQGAP1 bound with extensive actin in S1P-treated BMSCs. These results prove that S1P induces the combination between IQGAP1 and Cdc42/Rac1 in BMSCs.

Secondly, we analyzed the activation of Rho family in S1P-treated BMSCs. Pull-down assay indicated that S1P up-regulated the protein level of active GTP-bound Cdc42 and Rac1 (Figure 4B). By contrast, RhoA failed to be activated by S1P stimulation (Figure 4B). Simultaneously, the total Cdc42, Rac1, and RhoA protein levels were not affected by S1P treatment. To clarify functions of Cdc42 and Rac1 on BMSC motility, specific pharmacological inhibitors were used. Both MLS-573151 (Cdc42 inhibitor) and NSC-23766 (Rac1 inhibitor) restrained S1P-induced BMSC migration (Figure 4C). Thirdly, interactions of IQGAP1 and Cdc42/Rac1 were detected in S1P-treated BMSCs. The results of pull-down assays displayed that silencing IQGAP1 abrogated S1P-induced Cdc42 and Rac1 activation (Figure 4D). At the same time, IQGAP1 aggregation to the plasma membrane induced by S1P was impeded in the presentation of Cdc42- and Rac1-specific inhibitors, respectively (Figure 4E). In conclusion, Cdc42 and Rac1 activate IQGAP1 and influence subcellular localization of IQGAP1. On the other hand, IQGAP1 conjugates with Cdc42/Rac1 and stabilizes their active form. By this manner, IQGAP1 and Cdc42/Rac1 regulate BMSC motility in cooperation.

Silencing IQGAP1 in BMSCs significantly reduces the recruitment of BMSCs in MCDHF-diet-induced liver fibrosis

To identify whether IQGAP1 regulates BMSC motility *in vivo*, we manipulated a hydrodynamic intravenous injection of IQGAP1 siRNA to depress IQGAP1 expression in chimeric mice of BM cell labeled by EGFP. In previous study, hydrodynamic intravenous injection of siRNA, which is reported to transfer siRNA specifically to liver,[33] has been proven to result in siRNA uptake in liver, BM, kidney, and spleen.[34] Firstly, we confirmed the specificity of IQGAP1 knockdown. IQGAP1 expression was decreased by about 55% in mouse livers treated with IQGAP1 siRNA, especially in MCDHF diet feeding group (Figures 5A, 5E, and 5F). IQGAP1 expression of liver NPCs (including myofibroblasts of BMSC origin) were reduced (Figure 5A). We also employed flow cytometry to study IQGAP1 protein expression of NPCs. After

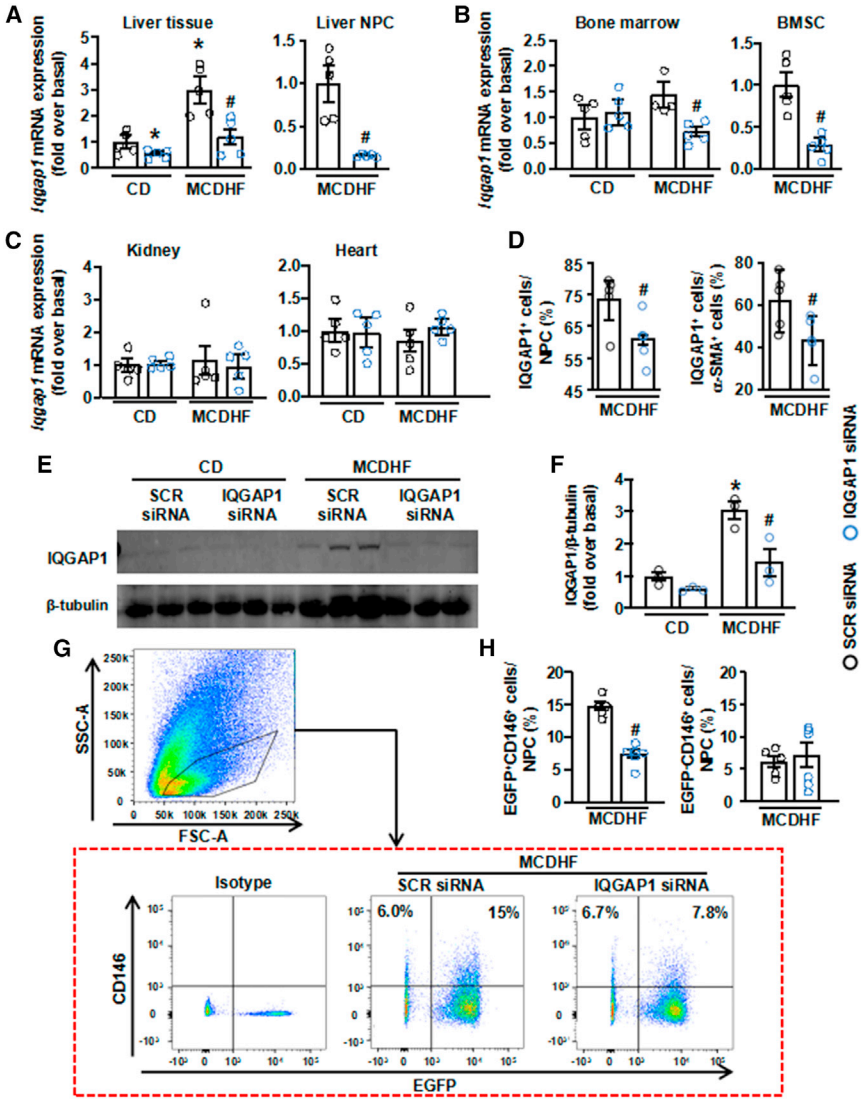

Figure 5. Silencing IQGAP1 significantly reduced the migration of BMSCs to the injured liver

(A and B) Mice injected with IQGAP1 siRNA were fed with MCDHF diet. The knockdown efficiency of liver and bone marrow was detected by qRT-PCR. (C) The mRNA expressions of *Iqgap1* in kidney and heart were also detected. (D) The percentage of IQGAP1$^+$ cells in NPCs or α-SMA$^+$ cells was examined by flow cytometry. (E) The protein level of IQGAP1 was studied in the mouse liver described above. (F) Quantification of IQGAP1 protein expression levels. (G and H) Liver NPCs were isolated from mouse liver with or without IQGAP1 knockdown. Flow cytometric analysis was used to examine the number of CD146$^+$, EGFP$^-$CD146$^+$, and EGFP$^+$CD146$^+$ cells in the fibrotic livers. The representative images of flow cytometric (G) and quantification of EGFP$^-$CD146$^+$ (H, left) and EGFP$^+$CD146$^+$ cells number (H, right) were shown. Data are presented as the means ± SEM. *p < 0.05 versus control group and #p < 0.05 versus MCDHF group with SCR siRNA (n = 5, per group).

IQGAP1 knockdown, the percentage of IQGAP1$^+$ cells was decreased in NPCs (from ~73% to ~60%), especially in α-SMA$^+$ cells (from ~62% to 43%), indicating the decrease of IQGAP1 protein expression in NPCs and α-SMA$^+$ cells (Figures 5D and S1E). In addition, BM IQGAP1 expression was down-regulated by IQGAP1-specific siRNA administration (Figure 5B). Subsequently, the IQGAP1 of BMSCs, which were purified by anti-CD146 microbeads from BM,[17] was also predominantly decreased with IQGAP1 siRNA treatment (Figure 5B). However, the *Iqgap1* mRNA expressions of heart and kidney had no significant change (Figure 5C).

Secondly, we recorded the effect of IQGAP1 on BMSC motility *in vivo*. BMSCs were marked with PE-CD146 (MSC marker) antibody for flow cytometry analysis. Results revealed that inhibiting IQGAP1 expression strikingly abrogated the recruitment of BMSCs (CD146$^+$EGFP$^+$) but failed to alter the number of non-BM-derived MSCs (CD146$^+$EGFP$^-$) in the fibrotic liver (Figures 5G and 5H). These results indicate that silencing IQGAP1 reduces BMSC liver recruitment. In addition, we further confirmed the results by evaluating the quantity of myofibroblasts. The results of qRT-PCR and western blot showed that α-SMA expression was decreased prominently by IQGAP1 knockdown in contrast to MCDHF-diet-fed mice (Figures 6A and 6B). Flow cytometry analysis results proved that the number of myofibroblasts (α-SMA$^+$) diminished by IQGAP1 siRNA administration (Figure 6C). Meanwhile, immunofluorescence results reveal that the number of EGFP$^+$α-SMA$^+$ cells (myofibroblasts of BMSCs origin) was approximately 75% of α-SMA$^+$ cells in liver of chimeric mice feeding with MCDHF diet (Figures 6D and 6E), suggesting that BMSCs were indeed one pivotal origin of myofibroblasts in MCDHF-diet-induced liver fibrosis. In addition, immunofluorescence results also showed that the number of myofibroblasts derived from BMSCs (EGFP$^+$α-SMA$^+$) was obviously decreased in MCDHF-diet-fed mice with IQGAP1 siRNA treatment (Figures 6D–6F). In conclusion, inhibiting IQGAP1 expression markedly blocks the migration of BMSCs to injured liver and down-regulates the number of myofibroblasts in injured liver of MCDHF-diet-feeding mice.

Blockage of IQGAP1 obviously attenuates MCDHF-diet-induced liver injury and fibrosis

We then examined whether IQGAP1 affects liver injury and fibrosis by regulating BMSC migration. The results of Sirius Red staining demonstrated that MCDHF-diet-induced collagen deposition was notably alleviated by IQGAP1 knockdown (Figures 7A and 7B). Furthermore, *Col1a1* and *Col3a1* mRNA expression were also

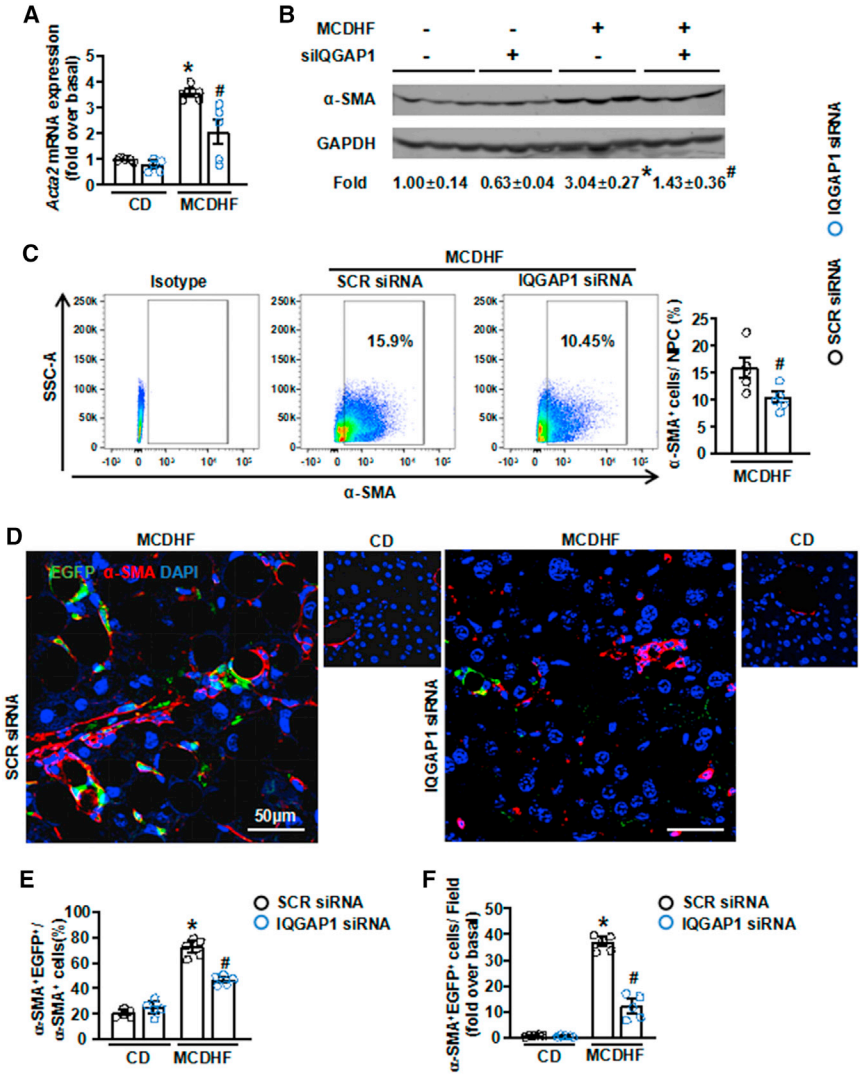

Figure 6. Silencing of IQGAP1 significantly reduced myofibroblasts in fibrotic liver

(A) The mRNA expression of *Acta2* was studied in MCDHF-diet-fed mouse liver after injecting SCR or IQGAP1 siRNA. (B) The protein level of α-SMA in MCDHF-diet-fed mouse liver after injecting SCR or IQGAP1 siRNAs. (C) Flow cytometric analysis was used to examine the number of α-SMA$^+$ cells in the fibrotic livers. The representative images of flow cytometric (left) and quantification of α-SMA$^+$ cells number (right) were shown. (D–F) The contribution of BMSCs to myofibroblasts was studied by immunofluorescence. The representative images (D) and quantification (E and F) of α-SMA$^+$ EGFP$^+$ cells were shown. DAPI: nuclear staining. Scale bars: 50 μm. Data are presented as the means ± SEM. *p < 0.05 versus control group and #p < 0.05 versus MCDHF group with SCR siRNA (n = 5, per group).

down-regulated in the livers with IQGAP1 siRNA treatment (Figures 7C and 7D). These results indicated that depressing IQGAP1 expression effectively attenuated liver fibrosis. In addition, the serum biochemical parameters of liver injury, including aspartate aminotransferase (AST) and alanine aminotransferase (ALT), were relieved by IQGAP1 siRNA in MCDHF-diet-treated mice (Figures 7E and 7F). Taken together, these results suggest that silencing IQGAP1 *in vivo* efficaciously alleviates liver injury and fibrosis induced by MCDHF diet via eliminating BMSC recruitment to damaged liver.

DISCUSSION

In the present research, we investigate the crucial role of IQGAP1 in BMSC migration and hepatic fibrosis. Our data demonstrate that IQGAP1 facilitates BMSC migration *in vitro* and *in vivo*. Furthermore, we determine the underlying mechanism of IQGAP1-mediated BMSC migration. S1P induces IQGAP1 membrane translocation in a $S1PR_3$-dependent manner and promotes the interplay between IQGAP1 and Cdc42/Rac1. *In vivo*, silencing IQGAP1 alleviates liver injury and fibrosis, suggesting that IQGAP1 is a potential therapeutic target for hepatic diseases (Figure 7G).

IQGAP1 was identified in 1994 for the first time.[35] A large number of disease-related studies have found that IQGAP1 affects the pathophysiological process of many organs and plays an important role in the occurrence and development of diseases, such as cancers, diabetic kidney disease, congenital heart disease, bronchial asthma, and multiple myeloma.[36–40] In liver, research on IQGAP1 mainly concentrates on HCC.[9,10] There are few studies about the function of IQGAP1 in liver fibrosis. In a recent study, IQGAP1, which is increased in CCl_4-induced mouse liver fibrosis, is reported to mediate inflammatory factor expression via affecting nuclear factor κB (NF-κB) signaling in TNF-α-treated LX-2 cells.[11] Our results also illustrate that IQGAP1 is increased in MCDHF-diet- or BDL-induced liver fibrogenesis and is positively correlated with fibrosis hallmarks. In addition, silencing IQGAP1 prominently prevents hepatic fibrosis induced by MCDHF diet. However, we found that IQGAP1 expression in S1P-treated BMSCs was not significantly increased. We speculate that the increase of IQGAP1 expression in liver may be caused by the increase of non-parenchymal cells with high IQGAP1 expression or the increase of IQGAP1 expression in non-parenchymal cells other than BMSCs, such as BM-derived macrophages (BMMs) (data not shown), during liver injury. In brief, this research reveals that IQGAP1 has considerable contribution to liver fibrosis, implicating that IQGAP1 may represent an effective therapeutic strategy of liver fibrogenesis.

The cell migration regulatory effect of IQGAP1 has been confirmed in several kinds of cells. For example, endothelial cells and vascular

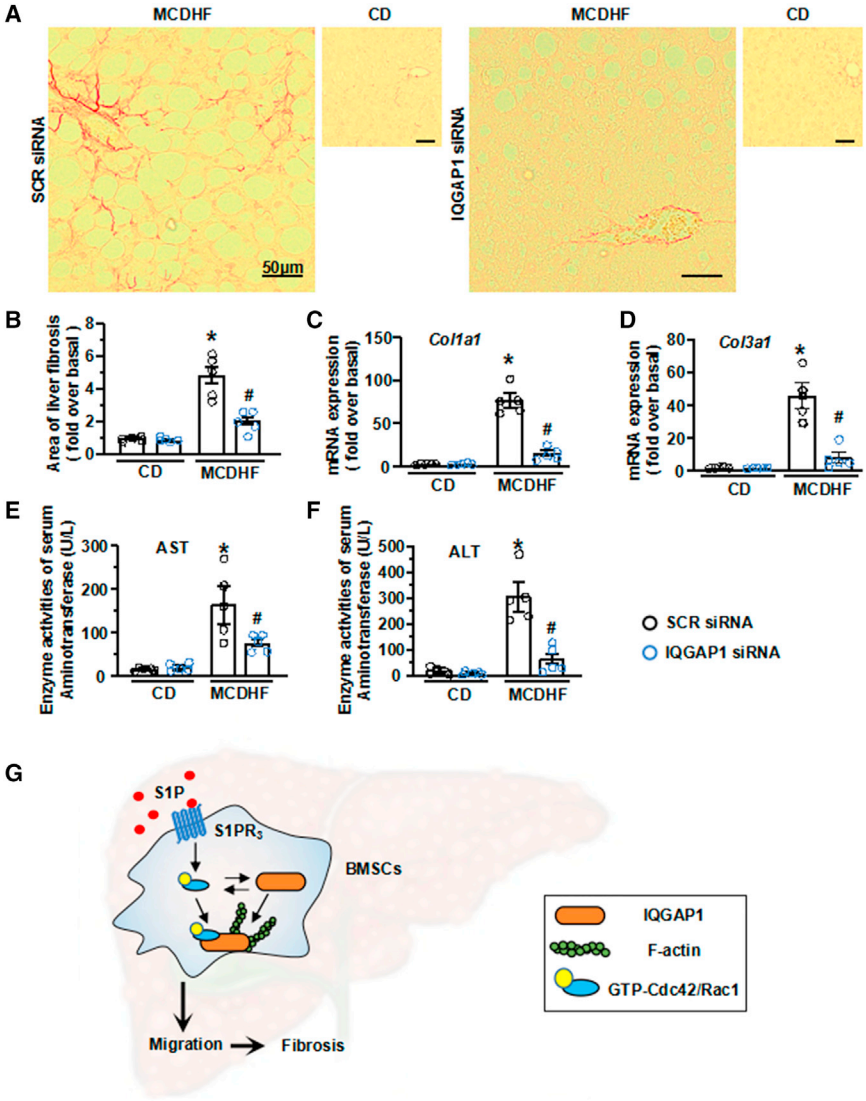

Figure 7. Silencing of IQGAP1 significantly attenuated MCDHF-induced liver injury and fibrosis

(A) Liver sections were subjected to Sirius Red staining. Scale bars: 50 μm. (B) The area of fibrotic liver was quantified. (C and D) mRNA levels of *Col1a1* (C) and *Col1a3* (D) were examined. (E and F) Serum levels of AST (E) and ALT (F) were measured in MCDHF-fed mice. (G) A schema diagram of IQGAP1-mediated, S1P-induced BMSC migration. Data are presented as the means ± SEM. *$p < 0.05$ versus control group and #$p < 0.05$ versus MCDHF group with SCR siRNA (n = 5, per group).

smooth muscle cells obtained from IQGAP1 knockout mice exhibit slow motility and proliferation.[41,42] IQGAP1 knockout mice also represent cardiovascular system defects due to impaired cell motility.[43,44] Moreover, IQGAP1 is essential in leukocytes migration across the endothelium.[45–48] Although the effect of IQGAP1 on cell migration has been studied in variety cell types, there are few reports about the effects of IQGAP1 on BMSC migration. This study explores regulatory functions of IQGAP1 in BMSC motility for the first time *in vivo* and *in vitro*.

In liver fibrogenesis, myofibroblasts are the main cells causing extracellular matrix deposition. Studies have shown that BMSCs, which recruited to injured liver, are a vital origin of myofibroblasts during MCDHF-diet-induced liver fibrogenesis (Figures 6D and 6E).[49,50] Our previous studies also discover that nearly 70% of myofibroblasts are derived from BMSCs in CCl_4-injured livers.[16] Therefore, investigations aimed at increasing our insight into the migration of BMSCs are essential to develop future therapeutic strategies. In our present research, results show that IQGAP1 siRNA treatment reduces BMSC motility *in vivo* and *in vitro*. On the other hand, we also studied whether IQGAP1 was involved in differentiation of BMSC to myofibroblasts *in vitro*. We treated BMSCs with transforming growth factor (TGF)-β1 and found that TGF-β1 did not affect IQGAP1 expression in BMSCs (Figure S2A), suggesting IQGAP1 was not involved in BMSC differentiation. Herein, our results prove that IQGAP1 reduces activated myofibroblast amount and alleviates liver fibrosis by blocking BMSC recruitment.

Previous studies have investigated that IQGAP1 participates in S1P-induced cell migration and adhesion of macrophages or endothelial cells.[51–54] For example, IQGAP1 modifies subcellular location in S1P-treated human pulmonary artery endothelial cells dependent on $S1PR_1$ and/or $S1PR_3$.[51] In macrophages, IQGAP1 is involved in $S1PR_2$-mediated actin translocation and phagocytosis.[53] In accordance with previous research, our results also identify that IQGAP1 is involved in S1P-induced BMSCs migration in a $S1PR_3$-dependent manner. In S1P-treated BMSCs, IQGAP1 achieves function by redistributing to cell periphery. What is more, S1P-induced IQGAP1 plasma membrane aggregation is blocked by specific $S1PR_3$ inhibitor and siRNA. In previous study, we have reported that S1P induces BMSC migration via $S1PR_3$ and HuR. HuR mRNA level was also studied in IQGAP1 knockdown BMSCs, and IQGAP1 did not affect HuR expression (Figure S2C).[26] On the other hand, these preceding articles have proven that IQGAP1 partakes in S1P-mediated cell functions by interacting with Rac1.[52,53] In our research, we prove that IQGAP1 affects BMSC migration by binding with not only Rac1 but also Cdc42. First, our results reveal that Cdc42 and Rac1 are involved in S1P-induced BMSC migration. Second, the interactions between IQGAP1 and Cdc42 and Rac1 are detected in S1P-treated cells. Third,

Cdc42 and Rac1 participate in S1P-induced membrane translocation of IQGAP1 during BMSC migration. Moreover, IQGAP1 regulates their activation in S1P-treated BMSCs. We consider the differences between our data and previous research might be caused by two reasons: (1) S1P activates distinct S1PRs in different cells and (2) the functions of extracellular and intracellular S1P are different since they trigger divergent signaling pathways.

In conclusion, we identify the indispensable function of IQGAP1 in promoting BMSC motility *in vitro* and *in vivo*. We also reveal the underlying mechanism of BMSC migration. What is the most important, we discover that silencing IQGAP1 alleviates the liver fibrosis by blocking BMSC migration to fibrotic liver. Our findings open new perspectives for the further hepatic fibrosis treatment targeting IQGAP1.

MATERIALS AND METHODS

Mouse models of liver injury

Liver injury models were induced by MCDHF diet (A06071309, Research Diet) or BDL. For MCDHF diet, adult Institute of Cancer Research (ICR) mice were fed 5 g/day and were sacrificed at 3, 7, 14, and 28 days after MCDHF diet feeding (n = 6 per group). For BDL-induced liver injury, mice were anesthetized to receive a midline laparotomy and then the common bile duct was exposed and ligated three times. Two ligatures were placed in the proximal portion of the bile duct, and one ligature was placed in the distal portion of the bile duct. The bile duct was then cut between the ligatures. Mice in sham group were exposed by laparotomy, but the common bile duct was not ligated. The mice were sacrificed at 1, 3, 7, and 14 days after operation (n = 6 per group).

To explore the role of IQGAP1 in BMSC migration *in vivo*, we prepared the chimeric murine model of BM cell labeled by EGFP. $EGFP^+$ BM cells were isolated from EGFP transgenic 3-week-old mice. ICR mice received lethal irradiation (8 Gy) and whole $EGFP^+$ BM cell (1.5×10^7 per mouse) transplantation by a tail vein injection. Four weeks later, mice of BM reconstruction received 2 weeks of MCDHF diet. At the same time, the mice received a hydrodynamic tail vein injection with IQGAP1 siRNA (1 μg/g body weight; CTM-438964, Dharmacon, Denver, CO) by invivofectamine 3.0 reagent (IVF3005, Invitrogen, Carlsbad, CA). Two weeks later, the livers were obtained for subsequent experiments.

All animal work was carried out under the ethical guidance of the ethics committee of Capital Medical University (AEEI-2019-049).

Human liver specimens

Human liver samples were obtained from 24 patients (12 men and 12 women; mean age 57 years; range 36–75 years) from snap-frozen surgical hepatectomy specimens. Liver samples (fibrosis stage: F2–F4) were collected from patients undergoing partial hepatectomy or liver transplantation. Fibrosis was related to autoimmune liver disease (n = 2), cholestatic cirrhosis (n = 2), cryptogenic cirrhosis (n = 3), Budd Chiari syndrome (n = 1), chronic hepatitis C virus (n = 4) or hepatitis B virus (n = 9) infections, and alcohol-induced liver disease (n = 3). All subjects gave their informed consent for inclusion before they participated in the study. The study was conducted in accordance with the Declaration of Helsinki, and the protocol was approved by the Ethics Committee of Beijing Shijitan Hospital, Capital Medical University, Beijing, China (project identification code: 2018EC-1).

Primary BMSC culture

The BM cells were flushed from the femur and tibia of 20 g ICR mice and were filtered through a 70-μm nylon mesh. Then, cells were washed by phosphate-buffered saline (PBS) containing 2% fetal bovine serum (FBS) and cultured with α-minimum essential medium (MEM) (Invitrogen) containing 20% FBS. The medium was all changed on the 2nd day and half changed on the 3rd day. After the first cell passage, the cells were cultured in α-MEM containing 15% FBS. Passages of 3–6 BMSCs were used for experiments. If not specifically stated, cells were collected after treatment with S1P (Cay62570-1, Biomol, Tebu, France) for 24 h, and CAY10444 ($S1PR_3$ inhibitor; 10,005,033, Cayman Chemical, Ann Arbor, MI), MLS-573151 (Cdc42 inhibitor; 0,453,647-3, Cayman Chemical), and NSC-23766 (Rac1 inhibitor; 0,441,977-5, Cayman Chemical) were added 1 h before the addition of S1P.

RNA interference

The siRNA targeting mouse IQGAP1 or $S1PR_3$ specifically was synthesized by Ambion (4,390,771 and 4,390,824, Carlsbad, CA). Transient transfection of siRNA (40 nmol/L) was performed by using Lipofectamine RNAiMAX (13,778-150, Invitrogen), as recommended by the manufacturer. Control cells were treated with 40 nmol/L SCR siRNA (Thermo Scientific). After 48 h, cells were used to perform subsequent experiments.

Cell migration assay

BMSC migration was determined using 8-μm Boyden chambers. Serum-starved BMSCs (4×10^4) were seeded to the upper chambers. S1P was added to the lower chambers. The chambers were incubated for 4 h at 37°C in 5% CO_2. BMSCs migrated to the lower face of porous plasma membrane were fixed with cold paraformaldehyde for 30 min and stained with hematoxylin for 1 h. Unmigrated BMSCs were removed with cotton swabs. Migrated BMSCs were photographed and quantified by cell counting.

Immunofluorescent staining

Liver samples were fixed in 4% paraformaldehyde for 48 h. After being dehydrated and embedded, the samples were cut into 5-μm slices. For preparation of hepatocytes and NPCs smear, isolated cells were fixed in 4% paraformaldehyde for 1 h. After permeabilization in PBS containing 0.5% Triton X-100 for 15 min, BMSCs were blocked with 2% BSA for 30 min. Primary antibodies of IQGAP1 (1:100; sc-376021, Santa Cruz Biotechnology, CA), α-SMA (1:100; ab32575, Abcam, Bristol, UK), and albumin (1:100, Santa Cruz Biotechnology) were used. Fluorescein isothiocyanate (FITC)- or Cy3-conjugated AffiniPure Goat Anti-Rabbit or -Mouse IgG (1:100; Jackson ImmunoResearch, PA) was used as secondary antibody.

Nuclei were stained with DAPI. The samples were observed under a confocal microscope (LSM510, Carl Zeiss MicroImaging, Jena, Germany).

F-actin staining and high-content assay

BMSCs (5×10^3) were plated in 96-well plates and treated with S1P for 1 h after starving 12 h. The cells were fixed in 4% paraformaldehyde for 30 min and washed with PBS three times. After permeabilization with Triton X-100, FITC-conjugated phalloidin (1:100; Molecular Probes, Eugene, OR) was used to stain F-actin for 20 min and nuclei were stained with DAPI. After washing the cells three times with PBS, the plate was imaged on a Thermo Scientific Cell Insight personal cell imaging platform (Thermo Fisher Scientific, Waltham, MA). Forty-nine fields were automatically acquired by the Thermo Scientific CellomicsiDEV software (Thermo Fisher Scientific, Waltham, MA). Cellomics Morphology Bio Application software (Thermo Fisher Scientific, Waltham, MA) was used to analyze the amount and distribution of F-actin of cells.

Detection of cell viability

BMSCs were transfected with IQGAP1 siRNA for 48 h. Cell viability was studied using CCK8 kit (Dojindo Molecular Technologies, Japan, DH6615).

qRT-PCR

Total RNA was extracted from liver specimens or cultured BMSCs using RNeasy mini kit (Qiagen, Germany). The quantity and purity of RNA was determined by NanoDrop 2000 spectrophotometer (Thermo Fisher Scientific). cDNA was synthesized using oligo (dT) and Moloney murine leukemia virus (M-MLV) reverse transcriptase (Invitrogen). qRT-PCR was performed with an ABI Prism 7300 sequence-detecting system (Life Technologies, Foster City, CA). Primers (Tianyi Biotech, Beijing, China) used for qRT-PCR were as follows: 18S rRNA, sense, 5′-GTAACCCGTTGAACCCCATT-3′, and anti-sense, 5′-CCATC CAATCGGTAGTAGCG-3′; human IQGAP1, sense, 5′-AGCTGCAG TCTGGAGTGGAT-3′, and anti-sense, 5′-CAGTGCTACTGCTGC CAATCT-3′; human ACTA2, sense, 5′-CCCTGAAGTACCCGATA GAACA-3′, and anti-sense, 5′-GGCAACACGAAGCTCATTG-3′; human COL1A1, sense, 5′-AGGTCCCCCTGGAAA-3′, and anti-sense, 5′-AATCCTCGAGCACCCTGA-3′; human COL3A1, sense, 5′-AGC TGGAAAGAGTGGTGACAG -3′, and anti-sense, 5′-CCTTGAGGA CCAGGAGCAC-3′; mouse *Iqgap1*, sense, 5′-GCCAGGAGAGACCT TGACTG-3′, and anti-sense, 5′-GCCCTCTGATGTTCAGCTTC-3′; mouse *Acta2*, sense, 5′-ATGCTCCCAGGGCTGTTTT-3′, and anti-sense, 5′-TTCCAACCATTACTCCCTGATGT-3′; mouse *Col1a1*, sense, 5′-AGGTCCCCCTGGAAAGAA-3′, and anti-sense, 5′-AAT CCTCGAGCACCCTGA-3′; mouse *Col3a1*, sense, 5′-AGCTGGAAA GAGTGGTGACAG-3′, and anti-sense, 5′-CCTTGAGGACCAGGA GCAC-3′; mouse *S1pr1*, sense, 5′-ACTTTGCGAGTGAGCTG-3′, and anti-sense, 5′-AGTGAGCCTTCAGTTACAGC-3′; mouse *S1pr2*, sense, 5′-TTCTGGAGGGTAACACAGTGGT-3′, and anti-sense, 5′-ACACCCTTTGTATCAAGTGGCA-3′; mouse *S1pr3*, sense, 5′-TC TCAGCCTTCATCCATTAACTCTAC-3′, and anti-sense, 5′-AGGGA GCCTTATGTCATACCACAA-3′; mouse *Actb*, sense, 5′-GGCTGT ATTCCCCTCCATCG-3′, and anti-sense, 5′-CCAGTTGGTAACAA TGCCATGT-3′; mouse *Cdc42*, sense, 5′-CCCATCGGAATATGTAC CAACTG-3′, and anti-sense, 5′-CCAAGAGTGTATGGCTCTCCA C-3′; mouse *Rac1*, sense, 5′-GAGACGGAGCTGTTGGTAAAA-3′, and anti-sense, 5′-ATAGGCCCAGATTCACTGGTT-3′; mouse *Elavl1*, sense, 5′-ATGCTGCTGAACAGACTTCG-3′, and anti-sense, 5′-TGTCTAATGGTTATGAAGACCACA-3′.

Western blot analysis

BMSCs were cultured in 10-cm tissue culture plates and treated with corresponding reagents. Radio-immunoprecipitation assay (RIPA) lysis buffer (R0010, Solarbio, Beijing, China) was used to prepare lysates. Fifty to one hundred micrograms of protein extracts were electrophoresed in 8% (for IQGAP1) or 12% (for α-SMA) SDS/polyacrylamide gels and transferred the protein to polyvinylidene fluoride (PVDF) membranes. The PVDF membranes were blocked with 5% nonfat milk at room temperature for 1 h. The blots were incubated with primary antibodies against IQGAP1 (1:1,000; sc-376021, Santa Cruz Biotechnology) or α-SMA (1:1,000; ab32575, Abcam), β-tubulin (1:5,000; HC101-01, Transgen Biotech, China), GAPDH (1:1,000; ab8245, Abcam), Cdc42 (1:1,000; 16,119, Thermo Scientific), Rac1 (1:167; 16,118, Thermo Scientific), or actin (1:2,000; Abcam). After 1 h incubation at room temperature with goat anti-rabbit IRDye-800-conjugated secondary antibody, goat anti-rabbit IRDye-700-conjugated secondary antibody, goat anti-mouse IRDye-800-conjugated secondary antibody, and goat anti-mouse IRDye-700-conjugated secondary antibody (1:10,000; 926–32,211, 926–68,021, 926–32,210, and 926–68,020, LI-COR Biosciences, Lincoln, NE), the signals were displayed using Odyssey Imaging System and quantified by the Odyssey v3.0 software (LI-COR Biosciences).

Cdc42, Rac1, and RhoA activation assay *in vitro*

Active Cdc42, Rac1, and RhoA were extracted using pull-down and detection kit as manufacturer's instruction (16,119, 16,118, and 16,116, Thermo Scientific). Active and total Cdc42, Rac1, and RhoA were shown by western blot.

Co-immunoprecipitation

Cells were lysed in NP-40 lysis buffer (supplemented with 1× proteinase inhibitor cocktail and 1 mM PMSF; P0013F, Beyotime Biotechnology, Beijing, China) by incubating on ice for 15 min, spin down cell debris, and nuclei by centrifugation at 12,000 g for 15 min at 4°C. Lysate was precleared by combining 10 μL of magnetic beads (10003D, Thermo Fisher Scientific, Waltham, MA) washed with lysis buffer, and the tube was incubated with gentle rotation for 30 min at 4°C. Then, the magnetic beads were discarded. An appropriate amount (1 to 2 μg) of IQGAP1 antibody (sc-376021, Santa Cruz Biotechnology) was added to the tube. Samples were incubated at 4°C for 2 h with gentle rotation. Subsequently, 20 μL magnetic beads (10003D, Thermo Fisher Scientific) were mixed with the samples and the samples were incubated with gentle rotation at 4°C overnight. The magnetic beads were

washed with lysis buffer five times and boiled with 2× SDS sample buffer at 100°C for 5 min. The immunocomplex was subjected to SDS-PAGE.

Non-parenchymal cells isolation and FACS

Livers were perfused with PBS twice and minced livers on the ice. Then, collagenase type IV was used to digest livers for 30 min at 37°C with gentle shaking. Digested extracts were filtrated through 70-μm cell strainers to obtain single-cell suspensions. The cell suspension was subjected to density gradient (Histopaque-1077 and 1119, Sigma-Aldrich, St. Louis, MO, USA) centrifugation at 2,000 rpm for 20 min. Cells were collected from the upper layer of the interface after centrifugation and washed twice with PBS. Cells were resuspended in PBS at 1.5×10^5 cells/100 μL. Then, PE-CD146 antibody (562,196, BD Bioscience, Franklin Lakes, NJ) or isotype-matched negative control antibody was added to the cell suspension, respectively. After 20 min of incubation in the dark, the cells were washed with PBS and subjected to fluorescence-activated cell sorting (FACS). For the detection of α-SMA and IQGAP1, antibodies against α-SMA (1:50; ab21027, Abcam) and IQGAP1 (1:10; ab133490, Abcam) were employed as primary antibodies. FITC-conjugated (1:1,000; A-11055, Invitrogen) and phycoerythrin (PE)-conjugated (1:10; 558,416, BD Bioscience) secondary antibodies were then used. FACS was performed on a FACSAria and analyzed with FACSDiva4.1 (BD Biosciences).

Primary hepatocyte isolation

Primary hepatocytes were isolated as previously described.[55] In brief, liver was perfused with 0.4% collagenase IV buffer and minced. Hepatocytes were separated using low-speed centrifugation and 40% Percoll density gradient centrifugation.

Immunomagnetic cell sorting

$CD146^+$ cells were purified from BM by using CD146 MicroBeads (130-092-007, Miltenyi Biotec, Bergisch Gladbach, Germany), according to the manufacturer's instructions. Cell sorting efficiency was further verified by flow cytometry.

Quantitative analysis of liver fibrosis and inflammation

Liver tissues were fixed in PBS containing 4% paraformaldehyde for 48 h and embedded in paraffin. Sections (5 μm thick) were stained with Sirius Red for collagen visualization and with H&E for liver histology. Computer-assisted image analysis with MetaMorph software (Universal Imaging, Downingtown, PA) was used to assess the necrotic area and fibrotic area. The average of 15 regions were randomly selected as the percentage of fibrotic or injured area in each sample.

Statistical analysis

Data were expressed as means ± SEM and were analyzed by Student's t test or ANOVA when appropriate. Correlation coefficients were assessed with the Pearson correlation coefficient. $p < 0.05$ was considered significant. All results were verified in at least three independent experiments.

SUPPLEMENTAL INFORMATION

Supplemental information can be found online at https://doi.org/10.1016/j.omtn.2021.12.020.

ACKNOWLEDGMENTS

This work was supported by grants from the National Natural Science Foundation of China (81770603 and 81430013).

AUTHOR CONTRIBUTIONS

Study concept and design, L.L. and N.C.; acquisition of data, Y.M., Y.L., F.L., C.D., L.H.,C.Q., and L.Y.; analysis and interpretation of data, Y.M., N.C., and L.L.; drafting of the manuscript, Y.M., N.C., and L.L.; funding acquisition, N.C. and L.L.; study supervision, L.L.

DECLARATION OF INTERESTS

The authors declare no competing interests.

REFERENCES

1. Mataraza, J.M., Briggs, M.W., Li, Z., Entwistle, A., Ridley, A.J., and Sacks, D.B. (2003). IQGAP1 promotes cell motility and invasion. J. Biol. Chem. *278*, 41237–41245.
2. Noritake, J., Watanabe, T., Sato, K., Wang, S., and Kaibuchi, K. (2005). IQGAP1: a key regulator of adhesion and migration. J. Cell Sci. *118*, 2085–2092.
3. Shannon, K.B. (2012). IQGAP family members in yeast, Dictyostelium, and mammalian cells. Int. J. Cell Biol. *2012*, 894817.
4. Brown, M.D., and Sacks, D.B. (2006). IQGAP1 in cellular signaling: bridging the GAP. Trends Cell Biol. *16*, 242–249.
5. White, C.D., Erdemir, H.H., and Sacks, D.B. (2012). IQGAP1 and its binding proteins control diverse biological functions. Cell Signal. *24*, 826–834.
6. Briggs, M.W., and Sacks, D.B. (2003). IQGAP proteins are integral components of cytoskeletal regulation. EMBO Rep. *4*, 571–574.
7. Bogatkevich, G.S., Ludwicka-Bradley, A., Singleton, C.B., Bethard, J.R., and Silver, R.M. (2008). Proteomic analysis of CTGF-activated lung fibroblasts: identification of IQGAP1 as a key player in lung fibroblast migration. Am. J. Physiol. Lung Cell. Mol. Physiol. *295*, L603–L611.
8. Wang, H., Ramshekar, A., Kunz, E., Sacks, D.B., and Hartnett, M.E. (2020). IQGAP1 causes choroidal neovascularization by sustaining VEGFR2-mediated Rac1 activation. Angiogenesis *23*, 685–698.
9. Liu, C., Billadeau, D.D., Abdelhakim, H., Leof, E., Kaibuchi, K., Bernabeu, C., Bloom, G.S., Yang, L., Boardman, L., Shah, V.H., et al. (2013). IQGAP1 suppresses TbetaRII-mediated myofibroblastic activation and metastatic growth in liver. J. Clin. Invest. *123*, 1138–1156.
10. Mo, C.F., Li, J., Yang, S.X., Guo, H.J., Liu, Y., Luo, X.Y., Wang, Y.T., Li, M.H., Li, J.Y., and Zou, Q. (2020). IQGAP1 promotes anoikis resistance and metastasis through Rac1-dependent ROS accumulation and activation of Src/FAK signalling in hepatocellular carcinoma. Br. J. Cancer *123*, 1154–1163.
11. Yang, J., Xu, C., Wu, M., Wu, Y., Jia, X., Zhou, C., Zhang, X., Ge, S., Li, Z., and Zhang, L. (2021). MicroRNA-124 inhibits hepatic stellate cells inflammatory cytokines secretion by targeting IQGAP1 through NF-kappaB pathway. Int. Immunopharmacol. *95*, 107520.
12. Chen, C.H., Chang, L.T., Tung, W.C., Chen, Y.L., Chang, C.L., Leu, S., Sun, C.K., Tsai, T.H., Tsai, I.T., Chang, H.W., et al. (2012). Levels and values of circulating endothelial progenitor cells, soluble angiogenic factors, and mononuclear cell apoptosis in liver cirrhosis patients. J. Biomed. Sci. *19*, 66.
13. Liu, Y.W., Chiu, Y.T., Fu, S.L., and Huang, Y.T. (2015). Osthole ameliorates hepatic fibrosis and inhibits hepatic stellate cell activation. J. Biomed. Sci. *22*, 63.
14. Bottcher, K., and Pinzani, M. (2017). Pathophysiology of liver fibrosis and the methodological barriers to the development of anti-fibrogenic agents. Adv. Drug Deliv. Rev. *121*, 3–8.

15. Higashi, T., Friedman, S.L., and Hoshida, Y. (2017). Hepatic stellate cells as key target in liver fibrosis. Adv. Drug Deliv. Rev. *121*, 27–42.

16. Li, C., Kong, Y., Wang, H., Wang, S., Yu, H., Liu, X., Yang, L., Jiang, X., Li, L., and Li, L. (2009). Homing of bone marrow mesenchymal stem cells mediated by sphingosine 1-phosphate contributes to liver fibrosis. J. Hepatol. *50*, 1174–1183.

17. Yang, L., Dong, C., Yang, J., Yang, L., Chang, N., Qi, C., and Li, L. (2019). MicroRNA-26b-5p inhibits mouse liver fibrogenesis and angiogenesis by targeting PDGF receptor-beta. Mol. Ther. Nucleic Acids *16*, 206–217.

18. Ishihara, S., Sato, T., Du, G., Guardavaccaro, D., Nakajima, A., Sawai, S., Kataoka, T., and Katagiri, K. (2020). Phosphatidic acid-dependent localization and basal de-phosphorylation of RA-GEFs regulate lymphocyte trafficking. BMC Biol. *18*, 75.

19. Li, C., Zheng, S., You, H., Liu, X., Lin, M., Yang, L., and Li, L. (2011). Sphingosine 1-phosphate (S1P)/S1P receptors are involved in human liver fibrosis by action on hepatic myofibroblasts motility. J. Hepatol. *54*, 1205–1213.

20. Park, S.M., Brooks, A.E., Chen, C.J., Sheppard, H.M., Loef, E.J., McIntosh, J.D., Angel, C.E., Mansell, C.J., Bartlett, A., Cebon, J., et al. (2021). Migratory cues controlling B-lymphocyte trafficking in human lymph nodes. Immunol. Cell Biol. *99*, 49–64.

21. Park, Y.J., An, H.T., Park, J.S., Park, O., Duh, A.J., Kim, K., Chung, K.H., Lee, K.C., Oh, Y., Lee, S., et al. (2020). Tyrosine kinase inhibitor neratinib attenuates liver fibrosis by targeting activated hepatic stellate cells. Sci. Rep. *10*, 14756.

22. Rodriguez, Y.I., Campos, L.E., Castro, M.G., Aladhami, A., Oskeritzian, C.A., and Alvarez, S.E. (2016). Sphingosine-1 phosphate: a new modulator of immune plasticity in the tumor microenvironment. Front. Oncol. *6*, 218.

23. McGinley, M.P., and Cohen, J.A. (2021). Sphingosine 1-phosphate receptor modulators in multiple sclerosis and other conditions. Lancet *398*, 1184–1194.

24. Nagahashi, M., Takabe, K., Terracina, K.P., Soma, D., Hirose, Y., Kobayashi, T., Matsuda, Y., Wakai, T., et al. (2014). Sphingosine-1-Phosphate transporters as targets for cancer therapy. Biomed. Res. Int. *2014*, 651727.

25. Wang, Y., Aoki, H., Yang, J., Peng, K., Liu, R., Li, X., Qiang, X., Sun, L., Gurley, E.C., Lai, G., et al. (2017). The role of sphingosine 1-phosphate receptor 2 in bile-acid-induced cholangiocyte proliferation and cholestasis-induced liver injury in mice. Hepatology *65*, 2005–2018.

26. Chang, N., Ge, J., Xiu, L., Zhao, Z., Duan, X., Tian, L., Xie, J., Yang, L., and Li, L. (2017). HuR mediates motility of human bone marrow-derived mesenchymal stem cells triggered by sphingosine 1-phosphate in liver fibrosis. J. Mol. Med. (Berl) *95*, 69–82.

27. Gao, H., Priebe, W., Glod, J., and Banerjee, D. (2009). Activation of signal transducers and activators of transcription 3 and focal adhesion kinase by stromal cell-derived factor 1 is required for migration of human mesenchymal stem cells in response to tumor cell-conditioned medium. Stem Cells *27*, 857–865.

28. Pollard, T.D., and Borisy, G.G. (2003). Cellular motility driven by assembly and disassembly of actin filaments. Cell *112*, 453–465.

29. Bolado-Carrancio, A., Rukhlenko, O.S., Nikonova, E., Tsyganov, M.A., Wheeler, A., Garcia-Munoz, A., Kolch, W., von Kriegsheim, A., and Kholodenko, B.N. (2020). Periodic propagating waves coordinate RhoGTPase network dynamics at the leading and trailing edges during cell migration. Elife *9*, e58165.

30. Wang, M., Niu, J., Gao, L., Gao, Y., and Gao, S. (2019). Zerumbone inhibits migration in ESCC via promoting Rac1 ubiquitination. Biomed. Pharmacother. *109*, 2447–2455.

31. Wang, X., Tang, P., Guo, F., Zhang, M., Yan, Y., Huang, M., Chen, Y., Zhang, L., and Zhang, L. (2019). mDia1 and Cdc42 regulate activin B-induced migration of bone marrow-derived mesenchymal stromal cells. Stem Cells *37*, 150–162.

32. Watanabe, T., Wang, S., Noritake, J., Sato, K., Fukata, M., Takefuji, M., Nakagawa, M., Izumi, N., Akiyama, T., and Kaibuchi, K. (2004). Interaction with IQGAP1 links APC to Rac1, Cdc42, and actin filaments during cell polarization and migration. Dev. Cell *7*, 871–883.

33. Zhang, G., Song, Y.K., and Liu, D. (2000). Long-term expression of human alpha1-antitrypsin gene in mouse liver achieved by intravenous administration of plasmid DNA using a hydrodynamics-based procedure. Gene Ther. *7*, 1344–1349.

34. Larson, S.D., Jackson, L.N., Chen, L.A., Rychahou, P.G., and Evers, B.M. (2007). Effectiveness of siRNA uptake in target tissues by various delivery methods. Surgery *142*, 262–269.

35. Weissbach, L., Settleman, J., Kalady, M.F., Snijders, A.J., Murthy, A.E., Yan, Y.X., and Bernards, A. (1994). Identification of a human rasGAP-related protein containing calmodulin-binding motifs. J. Biol. Chem. *269*, 20517–20521.

36. Hu, W., Wang, Z.X., Zhang, S., Lu, X., Wu, J.Y., Yu, K.Y., Ji, A., Lu, W., Wang, Z., Wu, J., et al. (2019). IQGAP1 promotes pancreatic cancer progression and epithelial-mesenchymal transition (EMT) through Wnt/beta-catenin signaling. Sci. Rep. *9*, 7539.

37. Liu, Y., Su, H., Ma, C., Ji, D., Zheng, X., Wang, P., Zheng, S., Wang, L., Wang, Z., and Xu, D. (2019). IQGAP1 mediates podocyte injury in diabetic kidney disease by regulating nephrin endocytosis. Cell Signal. *59*, 13–23.

38. Sevim Bayrak, C., Zhang, P., Tristani-Firouzi, M., Gelb, B.D., and Itan, Y. (2020). De novo variants in exomes of congenital heart disease patients identify risk genes and pathways. Genome Med. *12*, 9.

39. Tian, Y., Tian, X., Gawlak, G., O'Donnell, J.J., 3rd, Sacks, D.B., and Birukova, A.A. (2014). IQGAP1 regulates endothelial barrier function via EB1-cortactin cross talk. Mol. Cell. Biol. *34*, 3546–3558.

40. Zhou, F., Wang, D., Wei, W., Chen, H., Shi, H., Zhou, N., Wu, L., and Peng, R. (2020). Comprehensive profiling of circular RNA expressions reveals potential diagnostic and prognostic biomarkers in multiple myeloma. BMC Cancer *20*, 40.

41. Ikeda, S., Yamaoka-Toji, M., Hilenski, L., Patrushev, N.A., Anwar, G.M., Quinn, M.T., and Ushio-Fukai, M. (2005). IQGAP1 regulates reactive oxygen species-dependent endothelial cell migration through interacting with Nox2. Arterioscler. Thromb. Vasc. Biol. *25*, 2295–2300.

42. Kohno, T., Urao, N., Ashino, T., Sudhahar, V., Inomata, H., Yamaoka-Tojo, M., McKinney, R.D., Fukai, T., and Ushio-Fukai, M. (2013). IQGAP1 links PDGF receptor-beta signal to focal adhesions involved in vascular smooth muscle cell migration: role in neointimal formation after vascular injury. Am. J. Physiol. Cell Physiol. *305*, C591–C600.

43. Sbroggio, M., Bertero, A., Velasco, S., Fusella, F., De Blasio, E., Bahou, W.F., Silengo, L., Turco, E., Brancaccio, M., and Tarone, G. (2011). ERK1/2 activation in heart is controlled by melusin, focal adhesion kinase and the scaffold protein IQGAP1. J. Cell Sci. *124*, 3515–3524.

44. Sbroggio, M., Carnevale, D., Bertero, A., Cifelli, G., De Blasio, E., Mascio, G., Hirsch, E., Bahou, W.F., Turco, E., Silengo, L., et al. (2011). IQGAP1 regulates ERK1/2 and AKT signalling in the heart and sustains functional remodelling upon pressure overload. Cardiovasc. Res. *91*, 456–464.

45. Gonzalez, A.M., Cyrus, B.F., and Muller, W.A. (2016). Targeted recycling of the lateral border recycling compartment precedes adherens junction dissociation during transendothelial migration. Am. J. Pathol. *186*, 1387–1402.

46. Sullivan, D.P., Dalal, P.J., Jaulin, F., Sacks, D.B., Kreitzer, G., and Muller, W.A. (2019). Endothelial IQGAP1 regulates leukocyte transmigration by directing the LBRC to the site of diapedesis. J. Exp. Med. *216*, 2582–2601.

47. Watson, R.L., Buck, J., Levin, L.R., Winger, R.C., Wang, J., Arase, H., and Muller, W.A. (2015). Endothelial CD99 signals through soluble adenylyl cyclase and PKA to regulate leukocyte transendothelial migration. J. Exp. Med. *212*, 1021–1041.

48. Weber, E.W., Han, F., Tauseef, M., Birnbaumer, L., Mehta, D., and Muller, W.A. (2015). TRPC6 is the endothelial calcium channel that regulates leukocyte transendothelial migration during the inflammatory response. J. Exp. Med. *212*, 1883–1899.

49. Forbes, S.J., Russo, F.P., Rey, V., Burra, P., Rugge, M., Wright, N.A., and Alison, M.R. (2004). A significant proportion of myofibroblasts are of bone marrow origin in human liver fibrosis. Gastroenterology *126*, 955–963.

50. Russo, F.P., Alison, M.R., Bigger, B.W., Amofah, E., Florou, A., Amin, F., Bou-Gharios, G., Jeffery, R., Iredale, J.P., and Forbes, S.J. (2006). The bone marrow functionally contributes to liver fibrosis. Gastroenterology *130*, 1807–1821.

51. Berdyshev, E.V., Gorshkova, I., Usatyuk, P., Kalari, S., Zhao, Y.T., Pyne, N.J., Pyne, S., Sabbadini, R.A., Garcia, J.G., and Natarajan, V. (2011). Intracellular S1P generation is essential for S1P-induced motility of human lung endothelial cells: role of sphingosine kinase 1 and S1P lyase. PLoS One *6*, e16571.

52. Bhattacharya, M., Su, G., Su, X., Oses-Prieto, J.A., Li, J.T., Huang, X., Hernandez, H., Atakilit, A., Burlingame, A.L., Matthay, M.A., et al. (2012). IQGAP1 is necessary for pulmonary vascular barrier protection in murine acute lung injury and pneumonia. Am. J. Physiol. Lung Cell. Mol. Physiol. *303*, L12–L19.

53. Hou, J., Chen, Q., Zhang, K., Cheng, B., Xie, G., Wu, X., Luo, C., Chen, L., Liu, H., Zhao, B., et al. (2015). Sphingosine 1-phosphate receptor 2 signaling suppresses macrophage phagocytosis and impairs host defense against sepsis. Anesthesiology *123*, 409–422.

54. Usatyuk, P.V., He, D., Bindokas, V., Gorshkova, I.A., Berdyshev, E.V., Garcia, J.G., and Natarajan, V. (2011). Photolysis of caged sphingosine-1-phosphate induces barrier enhancement and intracellular activation of lung endothelial cell signaling pathways. Am. J. Physiol. Lung Cell. Mol. Physiol. *300*, L840–L850.

55. Xie, J., Yang, L., Tian, L., Li, W., Yang, L., and Li, L. (2016). Macrophage migration inhibitor factor upregulates MCP-1 expression in an autocrine manner in hepatocytes during acute mouse liver injury. Sci. Rep. *6*, 27665.